Pergamon

J. Aerosol Sci. Vol. 29, No. 3, pp. 357–374, 1998

Printed in Great Britain
0021-8502/98 $19.00 + 0.00

PII: S0021-8502(97)10008-8

LIDAR OBSERVATION OF SPHERICAL PARTICLES IN A −65° COLD CIRRUS OBSERVED ABOVE SODANKYLA (FINLAND) DURING S.E.S.A.M.E.

Massimo Del Guasta,*† Marco Morandi,* Leopoldo Stefanutti,* Stefano Balestri,* Esko Kyro,‡ Markku Rummukainen,‡ Rigel Kivi,‡ Vincenzo Rizi,§ Bernhard Stein,‖ Carsten Wedekind,‖ Bernd Mielke,‖ Renaud Matthey,¶ Valentin Mitev¶ and Mathilde Douard**

* Istituto Ricerca Onde Elettromagnetiche CNR, Florence, Italy
‡ FMI Sodankyla Observatory, Finland
§ Universita' l'Aquila, l'Aquila, Italy
‖ Freie Universitat Berlin, Berlin, Germany
¶ Observatoire Cantonal Neuchatel, Neuchatel, Switzerland
** Universite' Lyon I, Villeurbanne, France

(*First received* 28 *April* 1997; *and in final form* 18 *September* 1997)

Abstract—The absence of LIDAR depolarization in a polar cirrus observed above Sodankyla (Finland) showed the presence of spherical particles at −65°C. The presence of pure liquid water is excluded, since homogeneous freezing should occur at or above −40°C. The cirrus layer was detected at the tropopause, during the horizontal and vertical advection above northern Scandinavia of warm and wet oceanic air. Two alternative explanations are suggested, the first one involving the presence of large, deliquescent tropospheric CN, freezing at very low temperature, and the second one involving the presence of metastable, spherical ice-particles produced in the fast adiabatic cooling of the airmasses. The second hypothesis is less reasonable because the absence of depolarized LIDAR signal implies a strict cylindrical symmetry in the particles, a symmetry that is difficult to maintain during the freezing process. © 1998 Elsevier Science Ltd. All rights reserved

1. INTRODUCTION

It is widely accepted that cold cirrus are composed of ice particles, since pure water cannot exist as a liquid in the atmosphere below about −40°C. The homogeneous freezing rate of water droplets rapidly increases to (at least) $10^9\ cm^{-3}s^{-1}$ as the temperature drops to −40°C (Pruppacher and Klett, 1978; Heymsfield and Sabin, 1989; Hagen *et al.*, 1981; Anderson *et al.*, 1980; Sassen and Dodd, 1988); therefore, water droplets undergo fast freezing as the temperature approaches this threshold. Below about −40°C, freezing is so rapid that no supercooled water can survive long enough to be detected by cloud remote sensing. Also, while several theoretical and laboratory studies confirm this behavior for pure water and diluted solutions of tropospheric salts (DeMott and Rogers, 1990), spherical particles, supposed to be liquid, have seldom been observed in cirrus clouds as far as about −50°C (Sassen, 1992).

Multiwavelength, depolarization LIDAR is a very useful technique for hunting "unusual" cirrus clouds: the depolarized scattering of the linearly polarized laser light by aspherical particles is typical of frozen cirrus, while the complete absence of LIDAR depolarization is indicative of particles with a cylindrical symmetry around the vertical axis. This is possible both with optically isotropic, spherical particles and with sedimenting, horizontally-oriented ice plates. Cirrus clouds growing close to the cold polar tropopause, at the interface between two atmospheric regions with very different chemistry are a particularly interesting LIDAR hunting ground, where unusual nucleation processes can occur.

In this work, a −65°C cold, non-depolarizing cirrus layer observed at the tropopause during the 1994–1995 winter in Sodankyla (Finland) is analyzed, with the conclusion that

† Author to whom correspondence should be addressed.

spherical, optically isotropic particles larger than about 1 μm are responsible for the absence of depolarization in most of the layer. This conclusion implies unusual cloud microphysics, involving deliquescent liquid droplets containing large tropospheric CN.

2. THE MEASUREMENT

A multiwavelength depolarization LIDAR operated in Sodankyla (67.4°N, Finland) during the project "Measurement and Modeling of Ozone and Aerosol in the Northern Atmosphere" (MOANA) within the framework of the Second European Stratospheric Arctic and Midlatitude Experiment campaign (SESAME). This important campaign, supported by the EC, was carried out in the arctic region throughout the 1994–1995 arctic winter. The LIDAR system used in Sodankyla was basically similar to the one described by Stefanutti *et al.* (1992) and already used in 1992 during EASOE (European Arctic Stratospheric Ozone Experiment) on the same site. The system is based on a Nd:YAG laser emitting vertically at 532 and 355 nm (the two beams are linearly polarized), a 60 cm Cassegrain telescope with 1 mrad FOV, and a LeCroy acquisition system collecting all the signals simultaneously. Only the received 532 nm radiation is polarization-analyzed and split into a "parallel" (p) and a "perpendicular" (s) signal. The maximum height resolution is 7.5 m. The LIDAR system operated throughout the 1994–1995 winter.

20 high cirrus clouds were LIDAR-observed during SESAME. Almost all such clouds showed a rather uniform depolarization ratio within the cloud (in this work, depolarization is defined as the ratio between the aerosol perpendicular LIDAR backscattering β_s, and the parallel β_p one). Depolarization was in the 10–40% range, similar to what was observed with a similar LIDAR in Antarctica by Del Guasta *et al.* (1993) and in the Arctic by Del Guasta *et al.* (1994).

In one particular case, starting at 16 GMT on 12 February 1995, and lasting for about 20 min (before the arrival of low, thick clouds) a non-depolarizing layer at 10,000 m was observed.

In Fig. 1 (top), the time evolution of the vertical profile of the aerosol parallel backscattering (β_p) is shown for the whole upper troposphere, while the depolarization ratio ($\mathrm{Dep} = \beta_s/\beta_p$) is shown below in the same figure. A depolarizing cirrus is present between 7500 and 9500 m, showing a depolarization of up to about 15%. The presence of depolarization is indicative of the presence of aspherical (certainly frozen) particles. This "common" cirrus will be disregarded in the rest of this work.

The thin upper-layer visible at 10,000 m showed a zero depolarization, well below the Raleigh depolarization of the pure molecular atmosphere (1–2%).

3. INTERPRETATION OF THE LIDAR DATA

3.1. *Depolarization*

The depolarization ratio is a very popular quantity among LIDAR researchers, as is an extremely useful parameter for detecting the presence of aspherical particles in a cloud. Nevertheless, it represents a loss of information, because it reduces bi-dimensional information (β_s, β_p) to mono-dimensional information (Dep). For this reason, the direct interpretation of depolarization may be misleading when working with mixed-phase or inhomogeneous clouds.

In a cloud composed of both spherical (usually liquid) and aspherical (usually solid) particles, β_p is mainly given by the spherical component, while β_s is given by the aspherical part. It is obvious that the ratio between these two quantities (depolarization ratio) has a practical, but not a physical, meaning, as the ratio of optical quantities comes from different scattering media. Only with homogeneous clouds does the ratio have a physical meaning. For this reason, depolarization changes with the height or with the time in a cloud which nature is unknown may be interpreted either as a consequence of a change in the microphysical properties of aspherical particles in a homogeneous ice cloud, or as a change

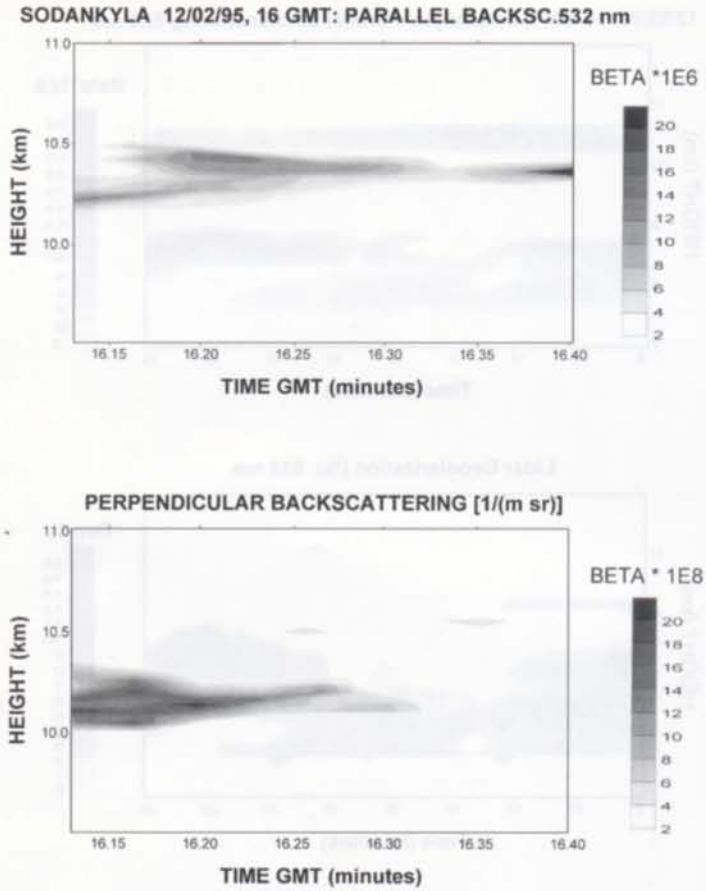

Fig. 1. Time evolution of the parallel backscattering (β_p) and the depolarization ratio in the upper troposphere. x-axis are minutes from 16:00 GMT. The layer at 10,000 m with no depolarization is to be noted.

in the ratio between aspherical and spherical particle populations in a inhomogeneus cloud. This ambiguity cannot be resolved by using the depolarization ratio alone. In such ambiguous cases, recovery of the aerosol backscattering data pair (β_s, β_p) is a fundamental step in avoiding most of these ambiguities.

In the present case study, a non-depolarizing layer was evidenced: spherical particles may have been responsible, but oriented plates could also have given a non-depolarized backscattering, like in the case fully described by Platt *et al.* (1978). In principle, atmospheric ice plates smaller than about 2 mm have the correct Reynolds numbers for showing an horizontal orientation during their free falling in the atmosphere (Lynch *et al.*, 1994). Even if ice plates (common in low cirrus) should be rare below $-30°C$ and with water subsaturation (Pruppacher and Klett, 1978; Chen and Lamb, 1994), 30–50 μm trigonal plates have been detected in high, $-83°C$ cold cirrus by Heymsfield (1986). The presence of horizontally-oriented ice plates cannot, thus, be excluded *a priori* in high cirrus, and in principle, may be responsible for the absence of depolarization in the 10,000 m-high-layer studied here. In our case, three physical considerations can contribute to exclude the hypothesis of oriented plates.

(1) The first consideration comes from Fig. 2, in which the aerosol LIDAR backscattering profiles β_s and β_p are shown for the cirrus layer at a height of 10,000–10,500 m. The absence of perpendicular backscattering in most of the cloud is striking. A single LIDAR profile of the same layer is indicated separately in Fig. 3, showing regions where no perpendicular signal at all was obtained from the cloud aerosol.

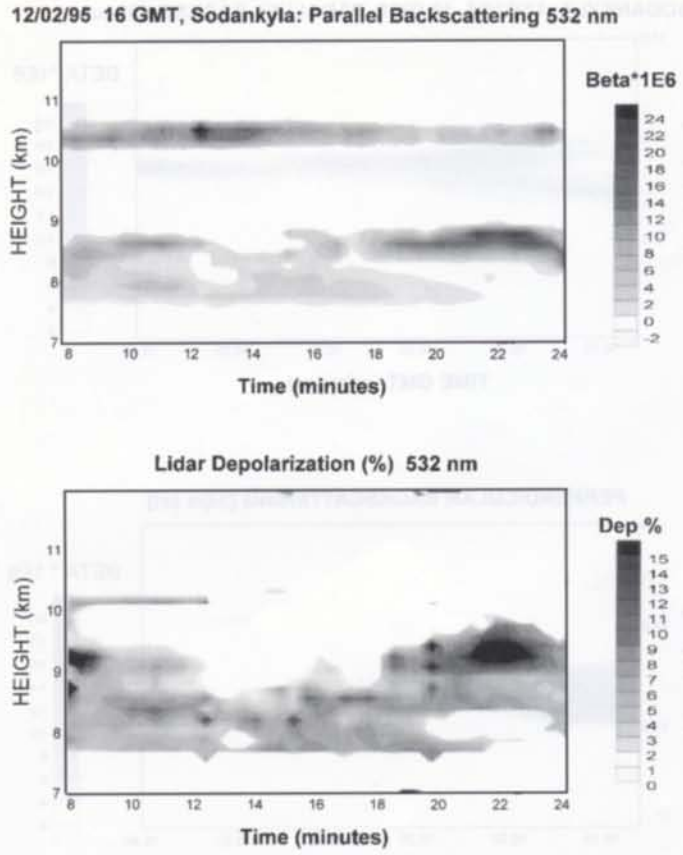

Fig. 2. Time evolution (as in Fig. 1) of the upper cirrus layer. Parallel and perpendicular LIDAR backscattering coefficients (β_p and β_s) are shown. The total absence of perpendicular backscattering from most of the cloud is to be noted.

In Fig. 4 a plot of β_s versus β_p for our case study is shown. Each point represents a 30 m vertical sample of the cloud, and all the cloud measurements have been included in the graph (points close to the axis origin ($\beta < 0.5\text{E-}6\ \text{m}^{-1}\,\text{sr}^{-1}$) are obviously affected by noise and by processing errors).

Two populations of particles are thus evidenced: a depolarizing (up to 10%) population and a non-depolarizing one. Two lines are shown that correspond to 2 and 10% constant depolarization. The non-depolarizing particles are well below the 2% depolarization line, corresponding approximately to the molecular depolarization observed in the pure air. These particles showed a depolarization of much less than 0.1%.

The estimated error on β_s and β_p due to processing errors is $\pm 0.5\text{E-}6\ \text{m}^{-1}\,\text{sr}^{-1}$ at 532 nm, and thus the relative error on depolarization is $0.5\text{E-}6/\beta_p$ if $\beta_p \gg 0.5\text{E-}6\ \text{m}^{-1}\,\text{sr}^{-1}$. This means that the depolarization values of less than 0.1% shown in Fig. 4 (with β_p of about $2\text{E-}6\ \text{m}^{-1}\,\text{sr}^{-1}$), are correct within $\pm 0.03\%$. In this work, we consider a depolarization of less than 0.1% as a complete absence of depolarization.

This is the most important key to excluding the presence of oriented plates, since clouds containing these plates give an almost zero depolarization ratio precisely because of an enhanced parallel backscattering (β_p) signal due to the specular reflection on the plates, and not because of the complete absence of a perpendicular signal. The parallel signal can be enhanced several orders of magnitude, and this way the depolarization ratio becomes reduced by the same factor, becoming squeezed to zero regardless to the presence of a depolarized signal. The oriented plates detected by Platt (1978) in a 3000 m high cloud, e.g. showed a very low but not negligible depolarization of about 1% in the backscattering when observed vertically, corresponding to an enhanced parallel beta of about

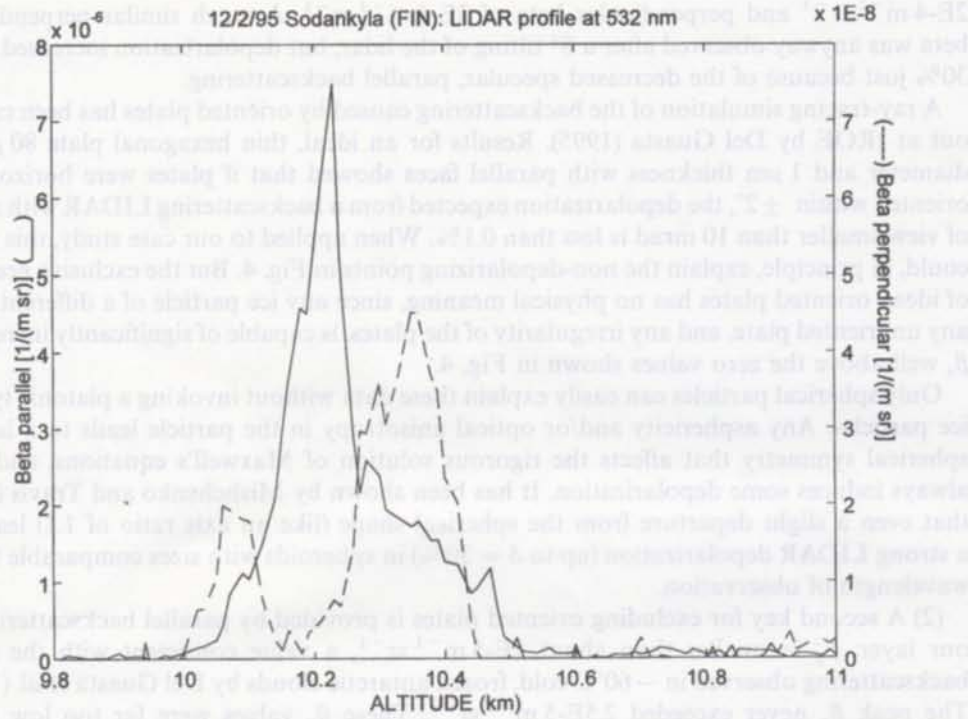

Fig. 3. Sample of the LIDAR backscattering vertical profile of the study layer. The thin line is the parallel backscattering profile; the thick one is 100 times the perpendicular backscattering. Units are $(m^{-1}\,sr^{-1})$.

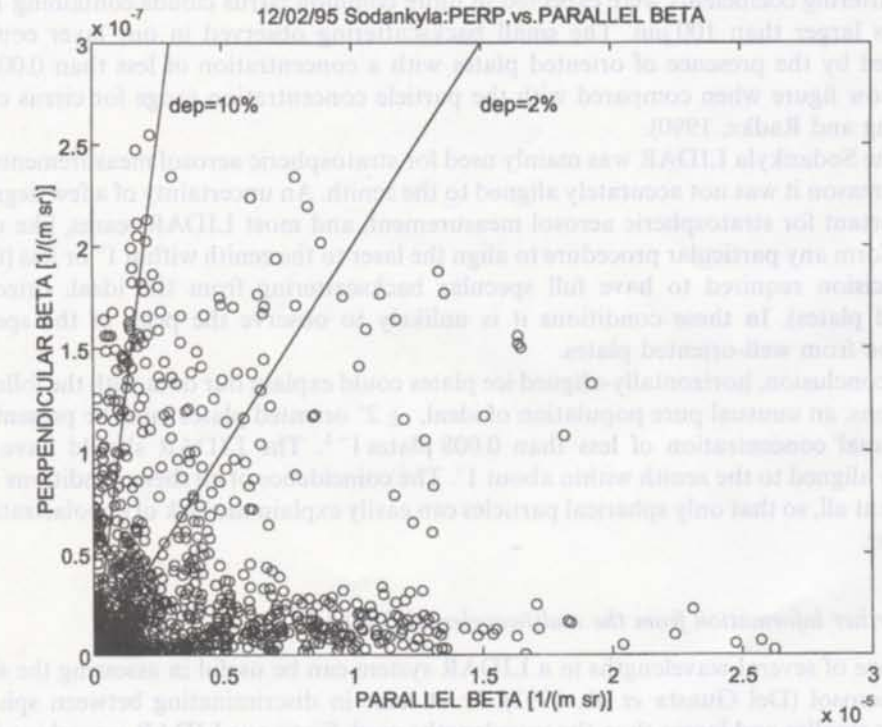

Fig. 4. Scatter plot of β_p and β_s for the whole cloud. Each point represents a 30 m slice of the LIDAR vertical profile. Two populations of particles are evidenced: a depolarizing (frozen) one and a liquid one. Iso-depolarization lines for 2% (Raleigh scattering) and 10% (frozen particles) are shown.

2E-4 $m^{-1} sr^{-1}$ and perpendicular beta of 2E-6 $m^{-1} sr^{-1}$. A much similar perpendicular beta was anyway observed after a 8° tilting of the lidar, but depolarization increased up to 30% just because of the decreased specular, parallel backscattering.

A ray-tracing simulation of the backscattering caused by oriented plates has been carried out at IROE by Del Guasta (1995). Results for an ideal, thin hexagonal plate 80 μm in diameter and 1 μm thickness with parallel faces showed that if plates were horizontally oriented within $\pm 2°$, the depolarization expected from a backscattering LIDAR with a field of view smaller than 10 mrad is less than 0.1%. When applied to our case study, this result could, in principle, explain the non-depolarizing points in Fig. 4. But the exclusive presence of ideal, oriented plates has no physical meaning, since any ice particle of a different kind, any unoriented plate, and any irregularity of the plates, is capable of significantly increasing β_s well above the zero values shown in Fig. 4.

Only spherical particles can easily explain these data without invoking a platonic type of ice particles. Any asphericity and/or optical anisotropy in the particle leads to a lack of spherical symmetry that affects the rigorous solution of Maxwell's equations, and thus always induces some depolarization. It has been shown by Mishchenko and Travis (1994) that even a slight departure from the spherical shape (like an axis ratio of 1.1) leads to a strong LIDAR depolarization (up to $\delta = 30\%$) in spheroids with sizes comparable to the wavelength of observation.

(2) A second key for excluding oriented plates is provided by parallel backscattering: in our layer, β_p is smaller than about 2E-5 $m^{-1} sr^{-1}$, a value consistent with the mean backscattering observed in −60°C cold, frozen antarctic clouds by Del Guasta *et al.* (1993). The peak β_p never exceeded 2.5E-5 $m^{-1} sr^{-1}$. These β_p values were far too low to be produced by oriented plates with a reasonable number concentration: in the presence of horizontally-oriented plates, in fact, the backscattering is strongly enhanced by specular reflection, as expected by Popov and Shefer (1994). A backscattering greater than 1E-3 $m^{-1} sr^{-1}$ (two magnitudes higher than our results) was expected also for clouds containing as few as 0.8 l^{-1} plates with a diameter of 37 μm. Three to four magnitudes larger backscattering coefficients were expected in more common cirrus clouds containing 10 l^{-1} particles larger than 100 μm. The small backscattering observed in our layer could be explained by the presence of oriented plates with a concentration of less than 0.008 l^{-1}, a very low figure when compared with the particle concentration range for cirrus clouds (Dowling and Radke, 1990).

(3) The Sodankyla LIDAR was mainly used for stratospheric aerosol measurements, and for this reason it was not accurately aligned to the zenith. An uncertainty of a few degrees is unimportant for stratospheric aerosol measurement, and most LIDAR teams, like us, do not perform any particular procedure to align the laser to the zenith within 1° or less (that is the precision required to have full specular backscattering from the ideal, orizonally oriented plates). In these conditions it is unlikely to observe the peak of the specular reflection from well-oriented plates.

As a conclusion, horizontally-aligned ice plates could explain our data with the following conditions: an unusual pure population of ideal, $\pm 2°$ oriented plates must be present with an unusual concentration of less than 0.008 plates l^{-1}. The LIDAR should have been casually aligned to the zenith within about 1°. The coincidence of all these conditions is not realistic at all, so that only spherical particles can easily explain the lack of depolarization in our layer.

3.2. *Further information from the multiwavelength LIDAR*

The use of several wavelengths in a LIDAR system can be useful in assessing the size of liquid aerosol (Del Guasta *et al.*, 1993), or at least in discriminating between spherical particles smaller and larger than the wavelengths used. Since our LIDAR is working in the visible region (355–532 nm), the discrimination between particles smaller or larger than about 1 μm is generally easy to perform. For the layer studied, every LIDAR profile was analyzed in order to compute the integrated backscattering throughout the cloud at

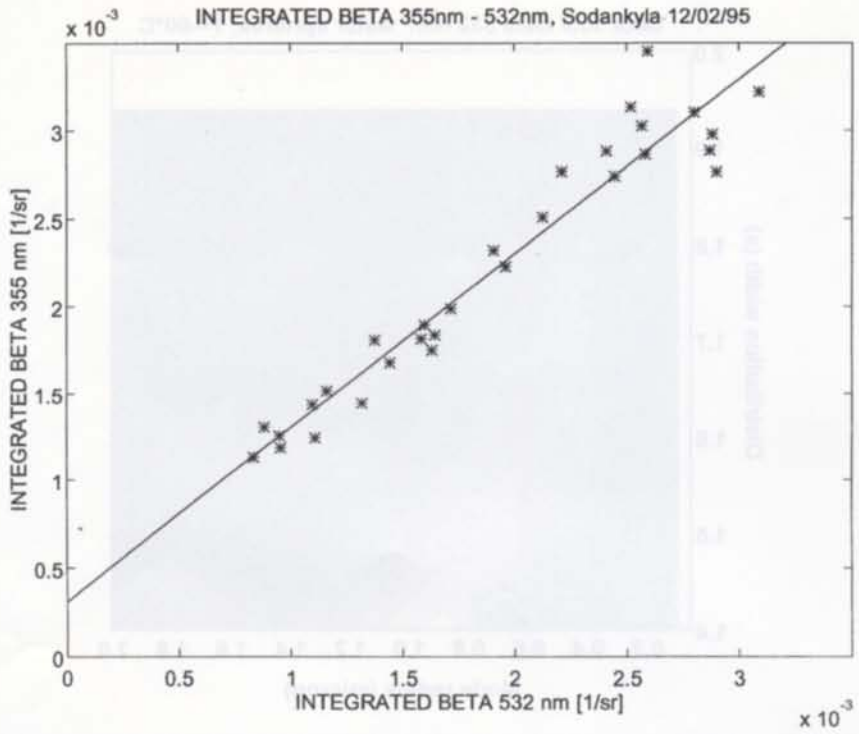

Fig. 5. Wavelength dependency of the cloud-integrated backscattering: Each point is obtained from a single LIDAR profile. A flat wavelength dependency is in evidence ($\beta_{532} = \beta_{355}$).

different wavelengths. In Fig. 5 the result is shown of such work for 532 and 355 nm. Each point was derived from a single LIDAR profile. The fitting line has a unitary slope, showing that the (integrated) backscattering was wavelength independent. Most of the layer was composed of spherical particles, so that the Mie theory can be applied in order to estimate the size magnitude of the particles. Fig. 6 shows the simulated ratio between β_{355} and β_{532} for liquid particles having a refractive index close to that of water, and with a lognormal size-distribution defined by

$$n(r) = N_t/(\sqrt{2\Pi}\, r \log(s)) \exp[-0.5(\log(r/r_m)/\log(s))^2]$$

(r_m is the mode radius, s is the distribution width, N_t is the total particle concentration).

X- and Y-axis in Fig. 6 are, respectively, the mode radius r_m and the adimensional width s of the lognormal distribution. The plot shows that β_{355}/β_{532} became close to 1 when the mode radius is larger than about 1.5 μm. Different chemical compositions of the droplets (ice, sulfuric acid, nitric acid) obviously, shifted this limit, but by a very limited amount. This estimation shows that the particles observed in the layer had to be larger than 1 μm mode radius to explain the multiwavelength LIDAR data.

In Fig. 7, the expected backscattering from a single water particle is reported, computed with the same conditions of Fig. 6. If the particle size is larger than 1 μm, as assessed, then the single-particle backscattering at 532 nm is larger than about (5–10)E-13 $m^{-1} sr^{-1}$. To explain the observed parallel backscattering of about 1E-5 $m^{-1} sr^{-1}$ for the particle population of Fig. 4, an upper limit of 20 particles cm^{-3} is then required.

Consequently, the number density of the particles in the layer should have been smaller than about 20 cm^{-3}.

3.3. *Meteorological information*

LIDAR data are often useless if good meteorological information is missing. During the SESAME campaign, the European Center for Midterm Weather Forecasting (ECMWF)

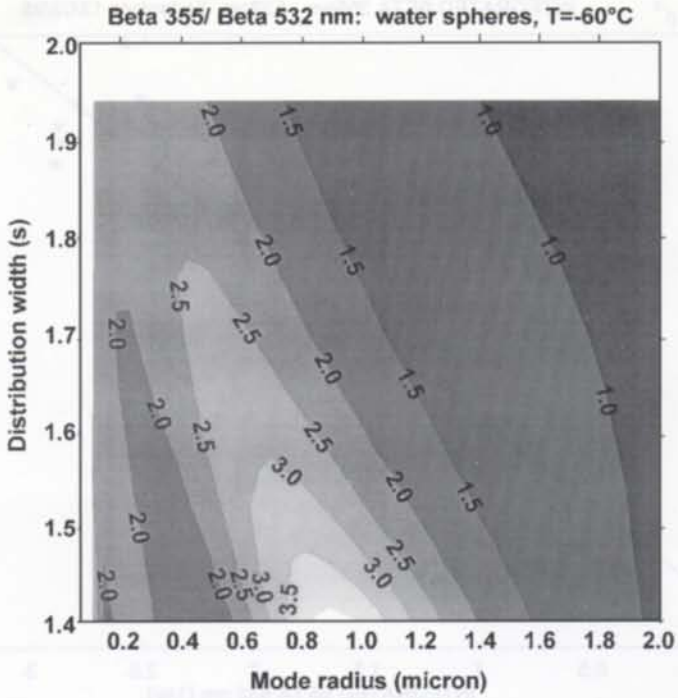

Fig. 6. Mie scattering simulation for droplets with refractive indeces close to those of water at −60°C. A lognormal size distribution is assumed. The ratio between β_{532} and β_{355} for a single droplet is shown for different mode radii and distribution widths. Particles larger than 1.5 μm show a flat wavelength dependency of the backscattering.

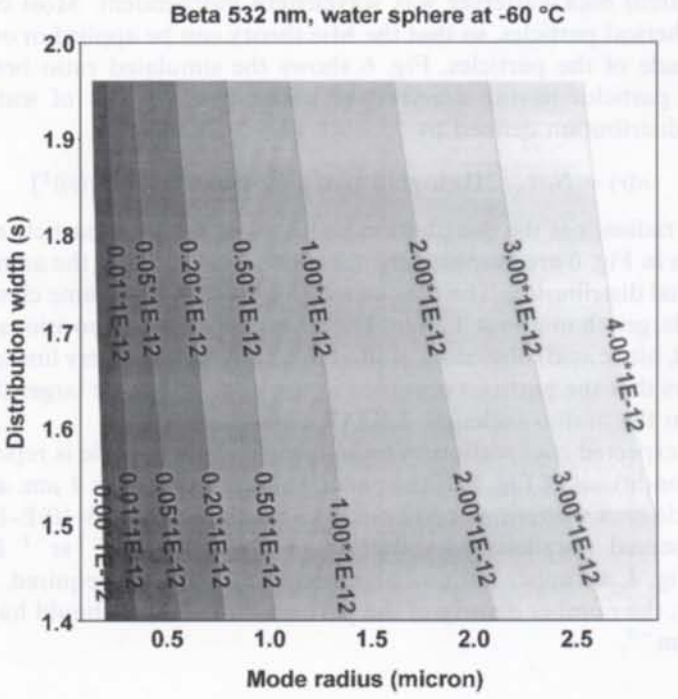

Fig. 7. Backscattering for single water droplet at −60°C, plotted as in Fig. 6.

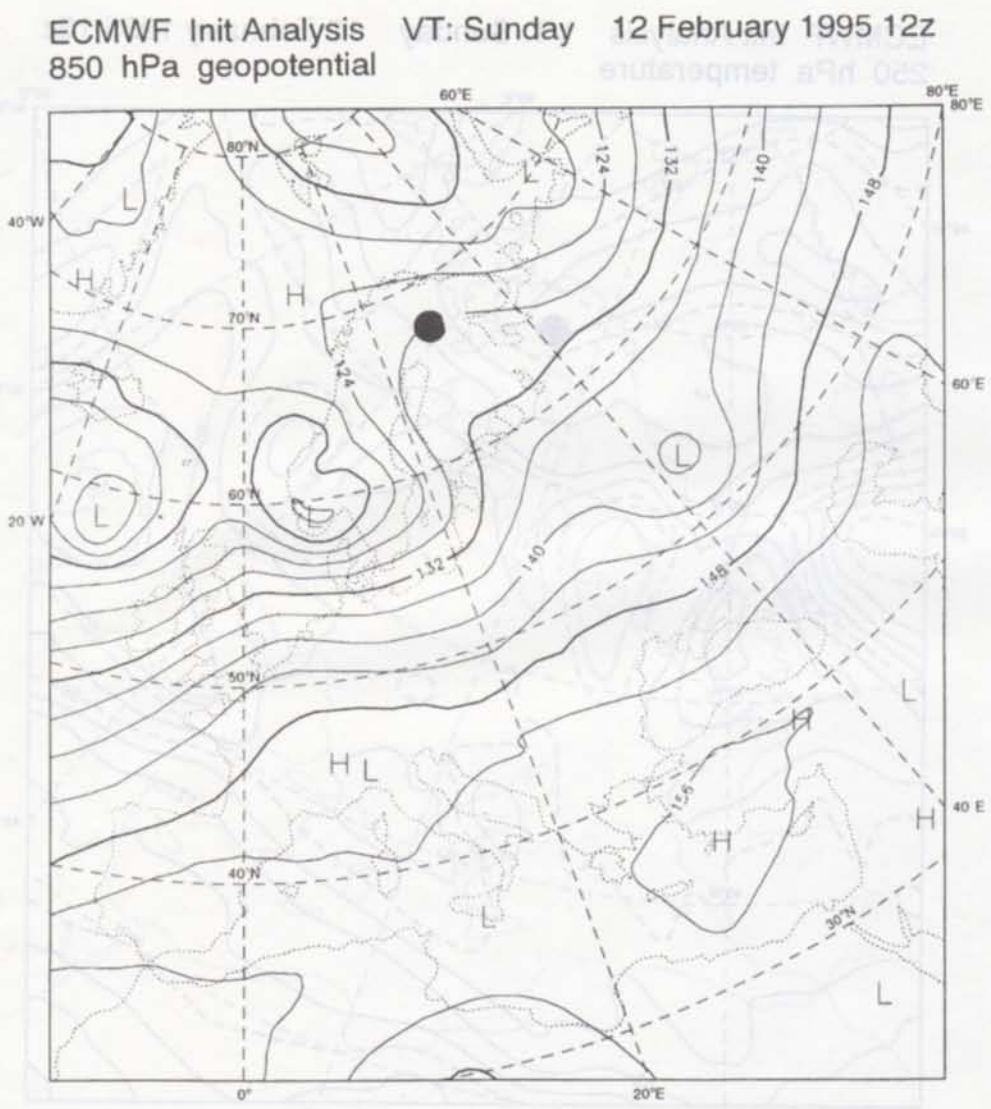

Fig. 8. Geopotential height analysis at 850 hPa for the measurement day at noon. A high-pressure ridge is evident above northern Scandinavia. A circle marks Sodankyla.

provided high-quality meteorological data for most of the Arctic region, so that the interpretation of LIDAR data was simplified. The 850 hPa geopotential height analysis for the study day at noon (4 h before the cloud event) is shown in Fig. 8. A high-pressure ridge was present over eastern Scandinavia, moving eastward. The lower stratosphere was adiabatically cooled above the ridge, showing on the analysis map (Fig. 9) temperatures colder than −65°C at 250 hPa above Lapland.

The thin cloud layer was observed at a height of 10,000–10,500 m, corresponding to a pressure level of 230–240 hPa and a potential temperature at cloud base/top of 310/315 K at 12 GMT, and 312/313 at 24 GMT, as derived from the two PTU soundings performed in Sodankyla at noon and midnight.

The ozone sounding performed in Sodankyla at 12 GMT together with the PTU sounding shows that, at that time, the thermal tropopause was very close (within a few hundred meters) to the sharp separation between the ozone-rich stratospheric air and the tropospheric air, poor in ozone. This means that, in this case, the thermal tropopause was very close to the dynamical tropopause. The dynamical tropopause (defined as the 1.6 PVU level by WMO (1985)), as computed from ECMWF data, was located at 10,200 m. The bulk

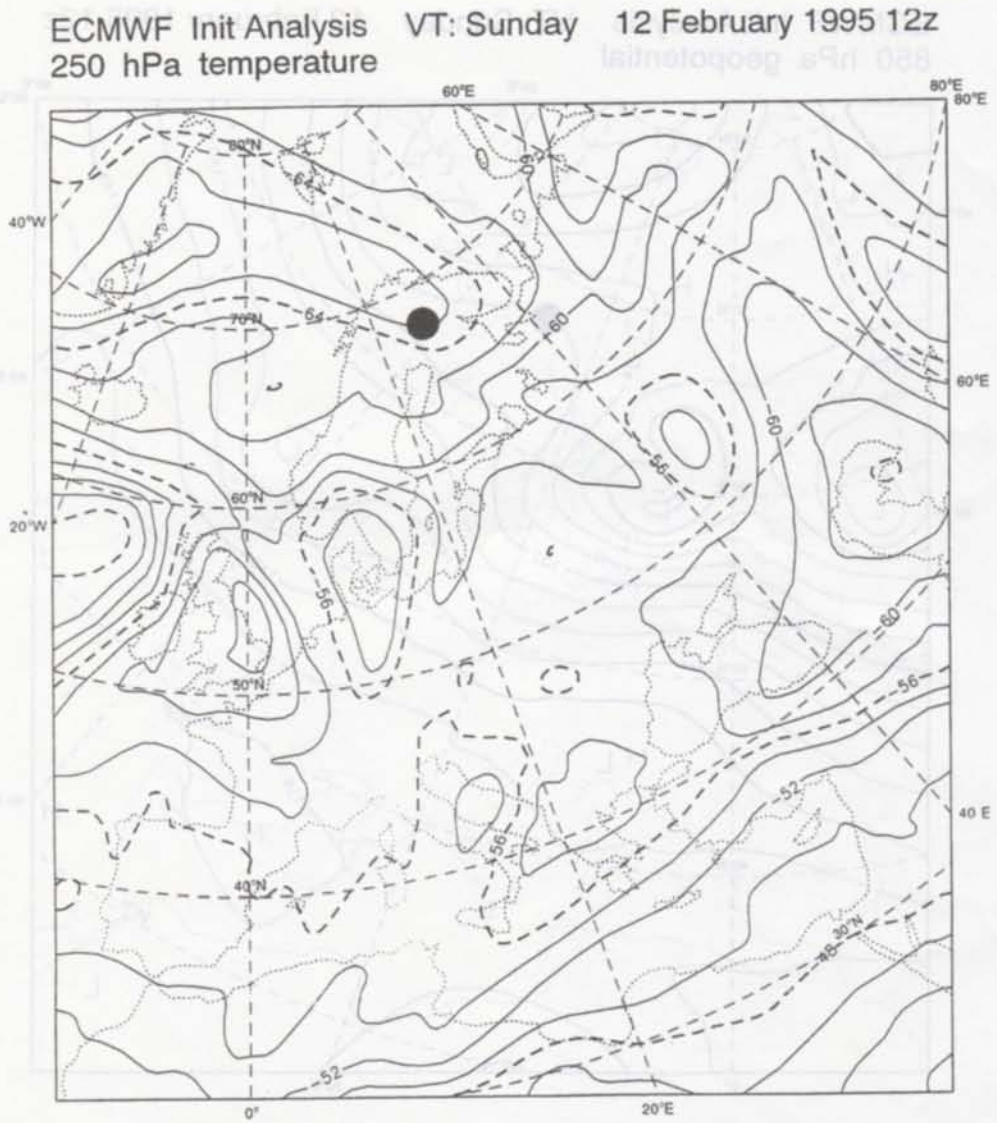

Fig. 9. Temperature analysis at 250 hPa, close to the study cloud level. A low-temperature region is shown above Northern Scandinavia. A circle marks Sodankyla.

Richardson number computed from PTU and wind data for the layer 10,000–10,500 m was 3.8 at 12 GMT, and increased to 150 at 24 GMT, showing that turbulence, and thus vertical exchange across the tropopause was unlikely to occur (Lee *et al.*, 1979).

The two temperature soundings are shown in Fig. 10. A warm air advection showing a warm front arrival is evident in the two temperature profiles between 5000 and about 10,500 m, with a temperature trend of +5°C/12 h above 5000 m. A corresponding adiabatic cooling of the lowest part of the stratosphere (10,500–12,000 m) below −70°C is also evidenced. The thermal tropopause moved up from 9500–10,000 m to 11,000 m. The dynamical tropopause moved to 10,500 m.

It is worth noting that the cloud layer studied was just below the boundary between these two regions. The temperatures of the layer bottom/top were −67°/−69°C in the PTU data of 12 GMT and −65°/−67°C at 24 GMT. Considering both the PTU data, the temperature in the cirrus layer was within the range −65°/−68°C.

The advecting air replaced the cold and dry air observed at 12 GMT (less than 30% RH with respect to liquid water above 5000 m, corresponding to less than 40% RH with respect

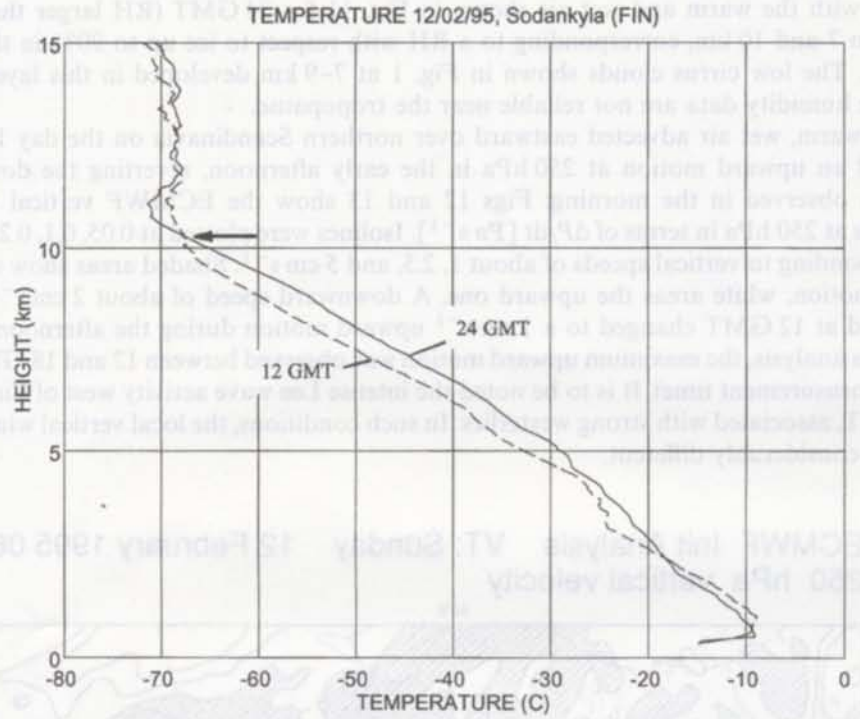

Fig. 10. Temperature soundings above Sodankyla on 12/2/95, at 12 GMT and 24 GMT (before and during the cloud observation). The advection of warm air between 5000 and 10,000 m is in evidence. An arrow marks the cloud height.

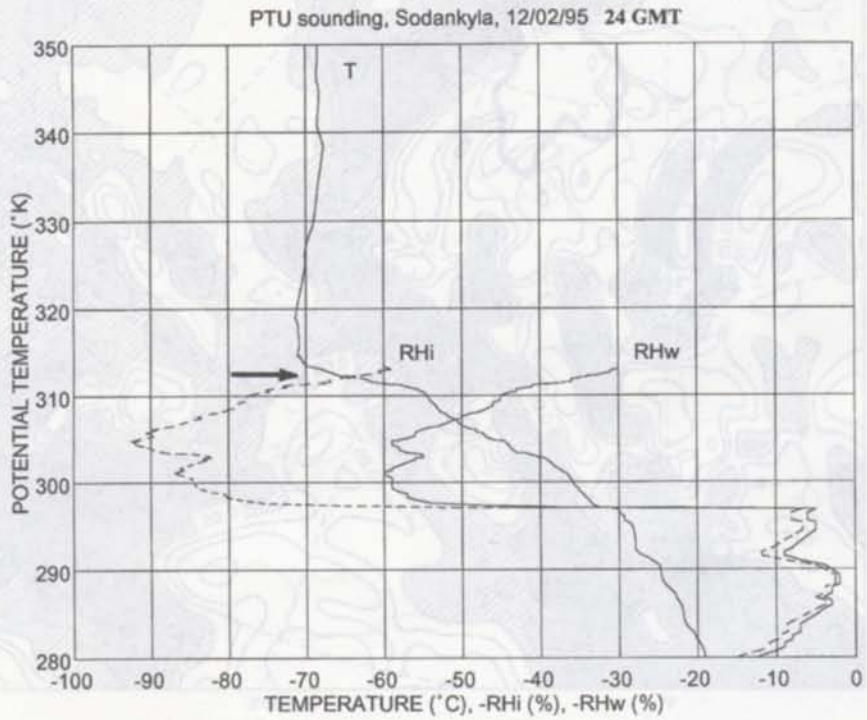

Fig. 11. Temperature and humidity plot for the 24 GMT sounding of 12 February. The cloud level is marked by arrows. Humidity is shown with respect to water (RHw) and ice (RHi). RH data are not reliable near or above the tropopause.

to ice) with the warm and wet air shown in Fig. 11 for 24 GMT (RH larger than 45% between 7 and 10 km, corresponding to a RH with respect to ice up to 90% in the same region). The low cirrus clouds shown in Fig. 1 at 7–9 km developed in this layer. PTU relative humidity data are not reliable near the tropopause.

The warm, wet air advected eastward over northern Scandinavia on the day 12/02/95 showed an upward motion at 250 hPa in the early afternoon, reverting the downward motion observed in the morning: Figs 12 and 13 show the ECMWF vertical velocity analysis at 250 hPa in terms of dP/dt [Pa s^{-1}]. Isolines were plotted at 0.05, 0.1, 0.2 Pa s^{-1}, corresponding to vertical speeds of about 1, 2.5, and 5 cm s^{-1}. Shaded areas show a downward motion, white areas the upward one. A downward speed of about 2 cm s^{-1} above Lapland at 12 GMT changed to a 1 cm s^{-1} upward motion during the afternoon. In the 250 hPa analysis, the maximum upward motion was observed between 12 and 18 GMT (the cloud measurement time). It is to be noted the intense Lee wave activity west of Finland at 18 GMT, associated with strong westerlies. In such conditions, the local vertical wind speed can be considerably different.

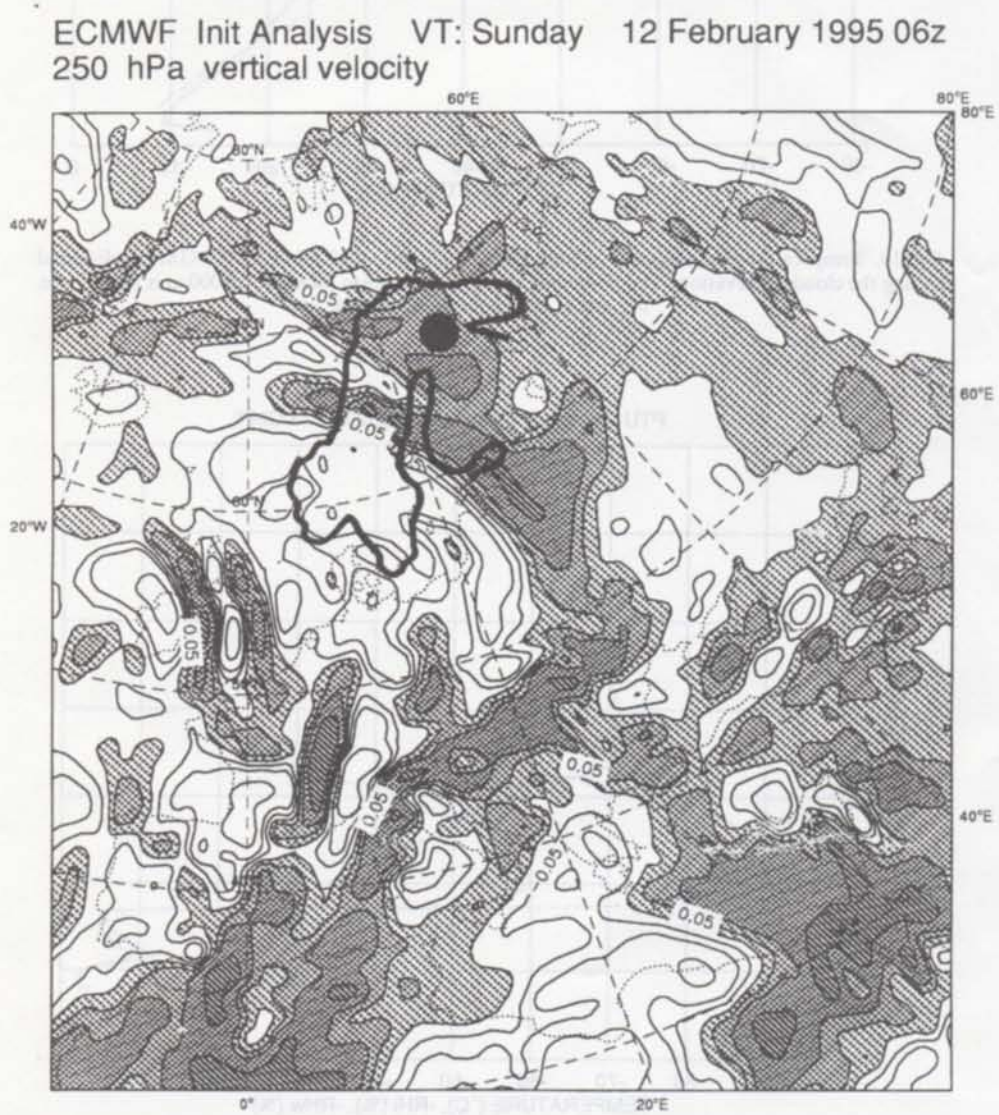

Fig. 12. Vertical velocity analysis from ECMWF for 6 GMT. Shaded areas are downward-motion regions; white regions show upward motion. Isolines are shown at 0.05, 0.1, 0.2 Pa s^{-1}. The Sodankyla station is marked with a circle.

Fig. 13. Vertical velocity analysis from ECMWF for 18 GMT. Shaded areas are downward motion regions; white regions show upward motion. Isolines are shown at 0.05, 0.1, 0.2 Pa s^{-1}. The Sodankyla station is marked with a circle.

3.4. *Trajectory analysis*

A trajectory analysis at the cloud level was performed in order to assess the origin of the air-mass. The air-mass trajectories were calculated with the KNMI (Royal Netherlands Meteorological Institute) 3-D trajectory model, using 6-hourly analysis data from ECMWF at T106 spectral resolution and at 31 model levels. The travel of an air mass arriving to the specified target pressure surface is traced backward in time by computing the lateral and vertical displacements in 2 h time steps interpolating ECMWF data in space and in time. The model has been tested out by Reiff *et al.* (1986) and Scheele *et al.* (1996). Trajectories were calculated backward starting from Sodankyla (230 hPa), for 11 February–13 February 1995. Results are shown in Fig. 14. Trajectories N° 1, 2, and 3 show the polar origin of air-masses before the cloud event. The vertical evolution of these three trajectories shows that within 5 d air masses were always in the 270–170 hPa region of the high troposphere. Trajectories 4 and 5, tracked after the cloud event, show a completely different air-mass origin. Air at 250 hPa was coming from SW, having spent 2–3 d over the Atlantic ocean.

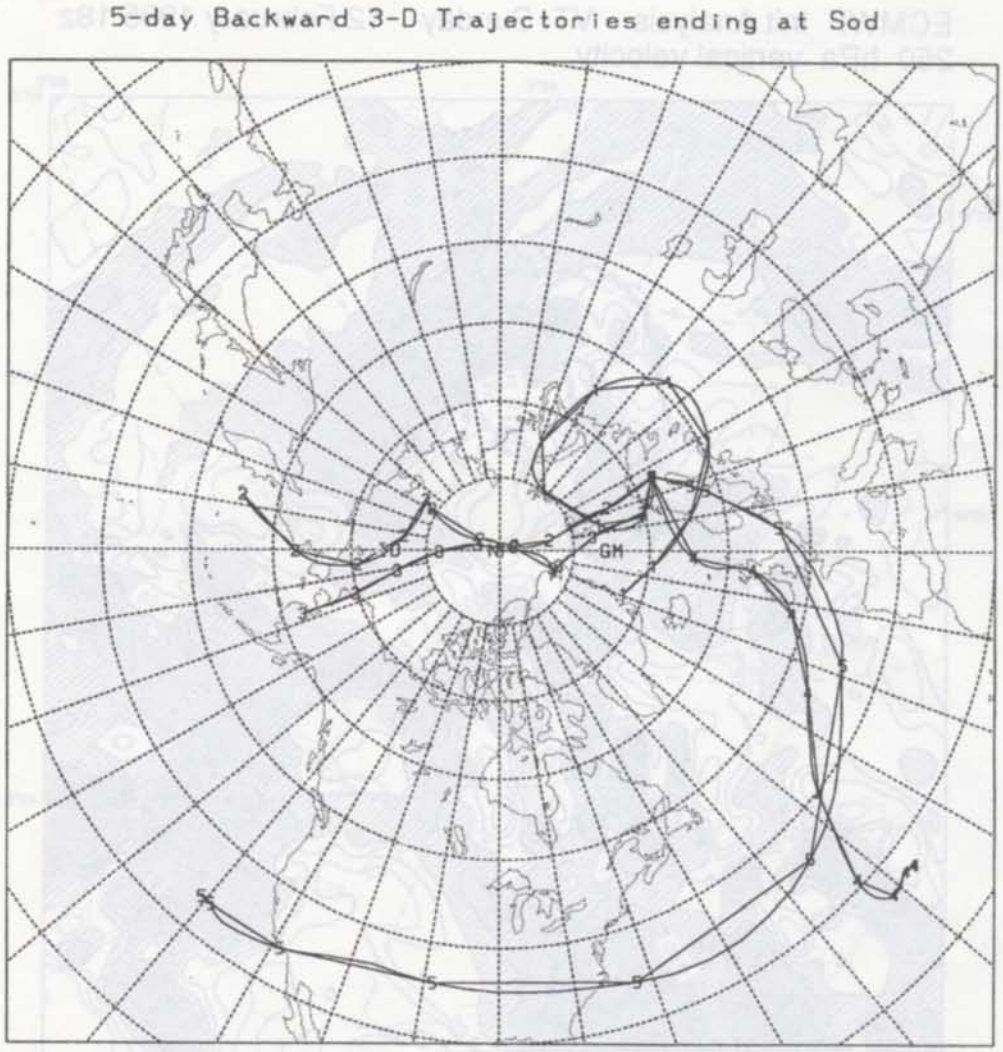

Fig. 14. Five backtrajectories with end point above Sodankyla at 230 hPa. Numbers were plotted every 12 h on each trajectory: (1) 11/02/1995 12 GMT; (2) 12/02/95 6 GMT; (3) 12/02/95 12 GMT; (4) 12/02/95 18 GMT; (5) 13/2/95 12 GMT.

The vertical evolution of these two trajectories shows that, a few days earlier, air was in the lower troposphere (500 hPa or less). The oceanic, low-level midlatitude origin of air-masses at 230 hPa meant that, at the layer level, contact between tropospheric wet air and very cold stratospheric air occurred.

3.5. *The end of the advected layer*

During the next day (13/2/95) at the 305–310 K level (8000–11,000 m), the advected warm, wet air became trapped in the stratosphere because of the advection of cold, dry air at 305 K (7000 m, Fig. 15). This cold advecting air slowly extended upward, mixing with the previously-advected warm air and restoring a relatively low (8000 m) and warm (-60°C) tropopause (Fig. 16).

The air that produced the cirrus layer thus became trapped in the stratosphere late on 13/2/95, showing a mechanism for the tropospheric–stratospheric exchange of water vapor and aerosols.

It is to be noted that, on 13 February the ELHYSA balloon flight performed above Kiruna (a Norvegian station upstream from Sodankyla at 300 K) showed an enhanced

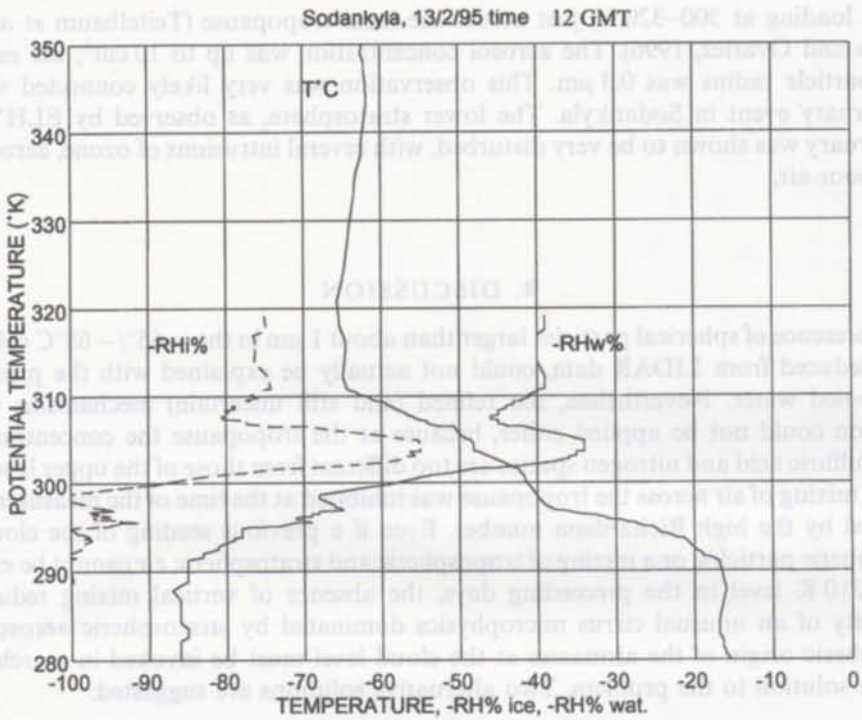

Fig. 15. Temperature and humidity plot for the 12 GMT sounding of 13, February 1 d after the cloud event. The PT cloud level is marked by arrows. Humidity (unreliable near the tropopause) is shown with respect to water (RHw) and ice (RHi).The advection of cold, dry air at 305°K is evident.

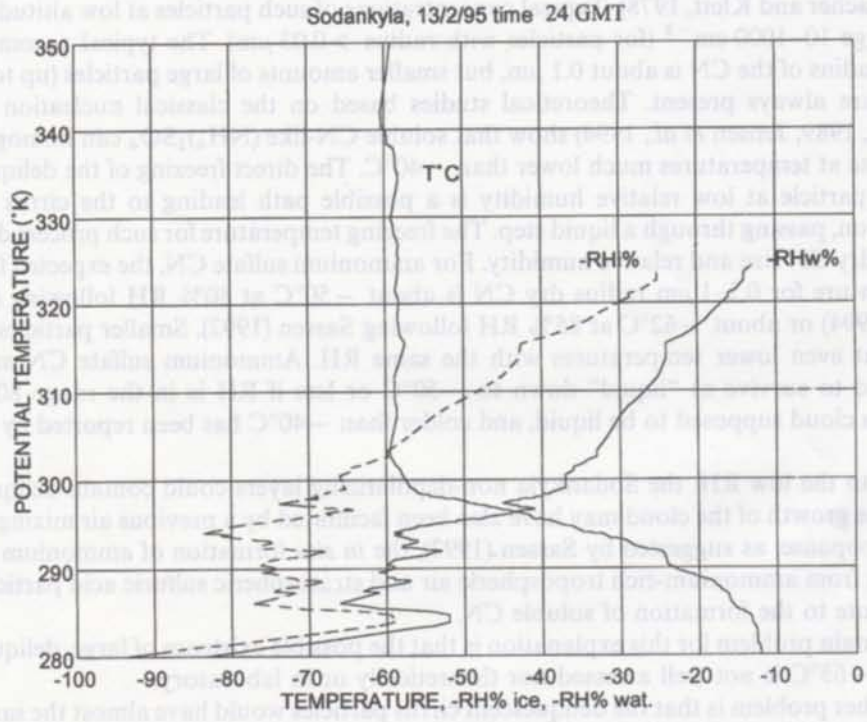

Fig. 16. Temperature and humidity plot for the 24 GMT sounding of 13 February. The cloud level is marked by arrows. Humidity is shown with respect to water (RHw) and ice (RHi). The cold air advection extended upward and restored a lower tropopause with compared to 12/2/95.

aerosol loading at 300–320 K, just across the local tropopause (Teitelbaum *et al.*, 1996; Ovarlez and Ovarlez, 1996). The aerosol concentration was up to 10 cm^3; the estimated mean particle radius was 0.3 μm. This observation was very likely connected with the 12 February event in Sodankyla. The lower stratosphere, as observed by ELHYSA on 13 February was shown to be very disturbed, with several intrusions of ozone, aerosol, and water-poor air.

4. DISCUSSION

The presence of spherical particles larger than about 1 μm in the $-65°/-68°$C cold study layer, deduced from LIDAR data, could not actually be explained with the presence of supercooled water. Nevertheless, the refined (and still uncertain) mechanisms of PSC formation could not be applied either, because at the tropopause the concentrations of water, sulfuric acid and nitrogen species are too different from those of the upper layers. The vertical mixing of air across the tropopause was inhibited at the time of the measurement, as indicated by the high Richardson number. Even if a previous seeding of the cloud with stratospheric particles, or a mixing of tropospheric and stratospheric air cannot be excluded at the 310 K level in the preceeding days, the absence of vertical mixing reduces the possibility of an unusual cirrus microphysics dominated by stratospheric aerosols. The tropospheric origin of the airmasses at the cloud level must be invoked in searching the possible solution to the problem. Two alternative solutions are suggested:

4.1. *Deliquescent particles*

Depending on the meteorological conditions, oceanic air masses contain variable amounts of soluble CN, mainly composed of $(NH_4)_2SO_4$ and other water-soluble sulfates (Pruppacher and Klett, 1978). Typical concentrations of such particles at low altitude are in the range 10–1000 cm^{-3} (for particles with radius >0.03 μm). The typical accomulation mode radius of the CN is about 0.1 μm, but smaller amounts of large particles (up to about 1 μm) are always present. Theoretical studies based on the classical nucleation theory (Sassen, 1989, Jensen *et al.*, 1994) show that soluble CN-like $(NH_4)_2SO_4$ can homogeneously freeze at temperatures much lower than $-40°$C. The direct freezing of the deliquescent sulfate particle at low relative humidity is a possible path leading to the cirrus crystal formation, passing through a liquid step. The freezing temperature for such process depends on the dry CN size and relative humidity. For ammonium sulfate CN, the expected freezing temperature for 0.1–1 μm radius dry CN is about $-50°$C at 80% RH following (Jensen *et al.*, 1994) or about $-62°$C at 85% RH following Sassen (1992). Smaller particles would freeze at even lower temperatures with the same RH. Ammonium sulfate CN are thus expected to survive as "liquid" down to $-50°$C or less if RH is in the range 80–85%. A cirrus cloud supposed to be liquid, and colder than $-40°$C has been reported by Sassen (1992).

Due to the low RH, the Sodankyla non-depolarizing layers could contain deliquescent CN. The growth of the cloud may have also been facilitated by a previous air mixing across the tropopause: as suggested by Sassen (1992), the *in situ* formation of ammonium sulfate starting from ammonium-rich tropospheric air and stratospheric sulfuric acid particles can contribute to the formation of soluble CN.

The main problem for this explanation is that the possible existence of large, deliquescent CN at $-65°$C is not well assessed nor theoretically or in laboratory.

Another problem is that the deliquescent cirrus particles would have almost the same size as the dry CN because of the low RH and temperature. This implies that large tropospheric aerosols (at least 1 μm radius) must have been transported in the upper troposphere. This was likely to occur in the frontal process described in this paper, but it is not a widely observed event.

4.2. *Ice spheres*

Even if liquid or liquid-coated particles could easily explain the sphericity of the observed aerosols, solid spheres cannot be excluded. Ice particles do not necessarily take on a regular, crystalline structure in the first stages of the growth process. It is possible that they assume a regular shape only later, when they reach several microns.

In Fig. 13, Lee wave activity is evident in the vertical wind analysis west of Finland. This kind of disturbance often produces orographic clouds above Sodankyla, due to the presence of the Norvegian Alps to the west. It is not possible to state the real presence of orographic waves above Sodankyla at the time of the measurement, but from Fig. 13 it can be stated that their presence was probable. In such case, the observed cirrus particles could have been spherical ice particles, produced because of the fast cooling rates associated with Lee waves. In this case, the ice particles would have had not time to reach a crystal shape in equilibrium with the vapor phase, and a metastable spherical shape could have been possible.

A big problem for this hypothesis is that ice particles must be very spherical (Section 3.1) and optically isotropic to give no depolarization. Crystalline ice is double-refractive, but the two refractive indexes are so close that an almost zero depolarization is expected from a perfect ice sphere with an internal, usual crystalline structure. On the other side, any optical or geometrical irregularity of the sphere (likely to be present in frozen particles) would introduce a measurable depolarization in the LIDAR return, as suggested in Section 3.1.

As a conclusion, the absence of LIDAR depolarization in the observed cloud is easy to explain only by invoking the presence of spherical, necessarily deliquescent particles. Neither oriented ice plates nor ice spheres are likely to represent a solution for the inverse scattering problem in this case. This conclusion implies an unusual microphysics for the studied polar cirrus, involving the presence of large, deliquescent CN preventing the freezing of the cloud droplets at a temperature as low as $-65°C$.

Acknowledgements—This work was supported by the European Commission, under contract EV5V CT930355 (M.O.A.N.A. project), and by the Programma Nazionale di Ricerche in Antartide (P.N.R.A.). We are very grateful to the Finnish Meteorological Institute (F.M.I.) for having hosted the LIDAR experiment in Sodankyla, and to the entire, friendly team of the Sodankyla station. We are also grateful to the European Center for Midrange Weather Forecasting (ECMWF) for the meteorological data, and to the Norvegian Meteorological Institute (KNMI) that supplied the model for the trajectory calculations.

REFERENCES

Anderson, R. J., Miller, R. C., Kassner, J. L. Jr. and Hagen, D. E. (1980) A study of homogeneous condensation-freezing nucleation of small water droplets in an expansion cloud chamber. *J. Atmos. Sci.* **37,** 2508–2520.

Chen Jen-ping and D. Lamb (1994) The theoretical basis for the parameterization of ice crystal habits: growth by vapor deposition. *J. Atmos. Sci.* **51**(9), 1206–1221.

Del Guasta, M., Morandi, M., Stefanutti, L., Brechet, J. and Piquard, J. (1993) One year of cloud lidar data from Dumont d'Urville: part I: General overview of geometrical and optical properties. *J. Geophs Res.* **98D10,** 18,575–18,587.

Del Guasta, M., Morandi, M., Stefanutti, L., Stein, B., Kolenda, J., Rairoux, P., Matthey, R. and Kyro, E. (1994) Multiwavelength lidar observation of thin cirrus at the base of the Pinatubo stratospheric layer during the EASOE campaign. *Geophys. Res. Lett.* **21**(13), 1339–1342.

Del Guasta, M. (1995) Calcolo delle proprieta' ottiche dei cristalli di ghiaccio mediante il metodo del tracciamento dei raggi. Applicazione al LIDAR a retrodiffusione; Technical Report IROE CNR, TR/GCF/95.04 [Available from IROE CNR Library, Via Panciatichi 64, 50127, Florence, Italy].

DeMott, P. J. and Rogers, D. C. (1990) Freezing nucleation rates of dilute solution droplets measured between $-30°$ and $-40°C$ in laboratory simulation of natural clouds. *J. Atmos. Sci.* **47**(9), 1056–1064.

Dowling, D. R. and Radke, L. F. (1990) A summary of the physical properties of cirrus clouds. *J. Appl. Meteorol.* **29,** 971–978,

Hagen, D. E., Anderson, R. J. and Kassner, J. L. Jr. (1981) Homogeneous condensation-freezing nucleation rate measurements for small water droplets in an expansion chamber. *J. Atmos. Sci.* **38,** 1236–1243.

Heymsfield, A. J. (1986) Ice particles observed in a cirriform cloud at $-83°C$ and implications for Polar stratospheric clouds. *J. Atmos. Sci.* **43**(8), 850–855.

Heymsfield, A. J. and Sabin, R. M. (1989) Cirrus crystal nucleation by homogeneus freezing of solution droplets. *J. Atmos. Sci.* **46**(14), 2252–2264.

Jensen, E. J., Toon, B. T., Westphal, D. L., Kinne, S. and Heymsfield, A. J. (1994) Microphysical modeling of cirrus 1. Comparison with 1986 FIRE IFO measurements. *J. Geophys. Res.* **99**(D5), 10,421–10,442.

Lee, D. R., Stull, R. B. and Irvine, W. S. (1979) Clear air turbolence forecasting techniques, AFGWC/TN-79/001. Air force Global Weather Central, Offutt AFB, NE 68113. 73 pp.
Lynch, K., Gedzelman, S. D. and Fraser, A. B. (1994) Subsuns, Bottlinger's rings, and elliptical halos. *Appl. Opt.* **33**(21), 4580–4589.
Michchenko, M. I. and Travis, L. D. (1994) Light scattering by polydispersions of randomly oriented spheroids with sizes comparable to wavelenght of observation. *Appl. Opt.* **33**(30), 7206–7225.
Ovarlez, J. and Ovarlez, H. (1996) Water vapour and aerosol measurements during SESAME, and the observation of low water vapour content layers. In *Polar Stratospheric Ozone* (Edited by J. A. Pyle, N. R. P. Harris and G. T. Amanatidis). Air Pollution Research Report 56, pp. 205–208. European Commission, Brussels.
Platt, C. M. R., Abshire, N. L. and McNice, G. T. (1978) Some microphysical properties of an ice cloud from LIDAR observation of horizontally oriented crystals. *J. Appl. Meteorol.* **17,** 1220–1224.
Popov, A. A. and Shefer, O. V. (1994) Theoretical and numerical investigation of the intensity of the LIDA signal specular reflected from a set of oriented ice plates. *Appl. Opt.* **33**(30), 7038–7044.
Pruppacher, H. R. and Klett, J. D. (1978) *Microphysics of Clouds and Precipitation.* Reidel, London, pp. 25–56.
Reiff, J., Forbes, G. S., Spieksma, F. T. M. and Reynders, J. J. (1986) African dust reaching northwestern Europe: a case study to verify trajectory calculations. J. Clim. Appl. Met. **25,** 1524–1567.
Sassen, K. and Dodd, G. C. (1988) Haze particle nucleation simulations in cirrus clouds, and applications for numerical and lidar studies. *J. Atmos. Sci.* **46**(19), 3005–3014.
Sassen, K. (1992) Evidence for liquid-phase cirrus cloud formation from volcanic aerosols: climatic implications. *Science* **257,** 516–519.
Scheele, M. P., Siegmund, P. C. and Velthoven, P. F. J. (1996) Sensitivity of trajectories to data resolution and its dependence on the starting point: in or outside a tropopause fold. *Meteorol. Appl.* **3,** 267–273.
Stefanutti, L., Castagnoli, F., Del Guasta, M., Morandi, M., Sacco, V. M., Venturi, V., Zuccagnoli, L., Kolenda, J., Kneipp, H., Rairoux, P., Stein, B. and Weidauer, D. (1992) A Four-wavelength depolarization backscattering LIDAR for polar stratospheric cloud monitoring. *Appl. Phys. B* **55,** 13–17.
Teitelbaum, H., Orvalez, J., Orvalez, H. and van Velthoven, P. (1996) Aerosol measurements during SESAME and its relationship with the polar vortex. In *Polar Stratospheric Ozone* (Edited by J. A. Pyle, N. R. P. Harris and G. T. Amanatidis). Air Pollution Research Report 56, pp. 149–153. European Commission, Brussels.
WMO (1995) *Atmospheric ozone 1985,* World Meteorological Organization, Global Ozone Research and Monitoring Project- Report No. 16.